Enhanced Magnetic Interaction between Ga and Fe in Two-Dimensional van der Waals Ferromagnetic Crystal Fe_3GaTe_2

Heming Zha(查鹤鸣)[1,2], Wei Li(李炜)[3], Gaojie Zhang(张高节)[4,5], Wenjing Liu(刘文晶)[1,2], Liwei Deng(邓力玮)[1,2], Qi Jiang(姜琦)[6], Mao Ye(叶茂)[1,2,7], Hao Wu(武浩)[4,5], Haixin Chang(常海欣)[4,5,8*], and Shan Qiao(乔山)[1,2,9*]

[1]*State Key Laboratory of Functional Materials for Informatics, Center for Excellence in Superconducting Electronics, Shanghai Institute of Microsystem and Information Technology, Chinese Academy of Sciences, Shanghai 200050, China*
[2]*Center of Materials Science and Optoelectronics Engineering, University of Chinese Academy of Sciences, Beijing 100049, China*
[3]*Department of Physics and State Key Laboratory of Surfac Physics, Fudan University, Shanghai 200433, China*
[4]*State Key Laboratory of Material Processing and Die & Mold Technology, School of Materials Science and Engineering, Huazhong University of Science and Technology, Wuhan 430074, China*
[5]*Wuhan National High Magnetic Field Center and Institute for Quantum Science and Engineering, Huazhong University of Science and Technology, Wuhan 430074, China*
[6]*Center for Transformative Science, ShanghaiTech University, Shanghai 201210, China*
[7]*Shanghai Synchrotron Radiation Facility, Shanghai Advanced Research Institute, Chinese Academy of Sciences, Shanghai 201210, China*
[8]*Shenzhen R&D Center of Huazhong University of Science and Technology, Shenzhen 518000, China*
[9]*School of Physical Science and Technology, ShanghaiTech University, Shanghai 201210, China*

(Received 13 May 2023; accepted manuscript online 12 July 2023)

Fe_3GaTe_2, a recently discovered van der Waals ferromagnetic crystal with the highest Curie temperature and strong perpendicular magnetic anisotropy among two-dimensional (2D) magnetic materials, has attracted significant attention and makes it a promising candidate for next-generation spintronic applications. Compared with Fe_3GeTe_2, which has the similar crystal structure, the mechanism of the enhanced ferromagnetic properties in Fe_3GaTe_2 is still unclear and needs to be investigated. Here, by using x-ray magnetic circular dichroism measurements, we find that both Ga and Te atoms contribute to the total magnetic moment of the system with antiferromagnetic coupling to Fe atoms. Our first-principles calculations reveal that Fe_3GaTe_2 has van Hove singularities at the Fermi level in nonmagnetic state, resulting in the magnetic instability of the system and susceptibility to magnetic phase transitions. In addition, the calculation results about the density of states in ferromagnetic states of two materials suggest that the exchange interaction between Fe atoms is strengthened by replacing Ge atoms with Ga atoms. These findings indicate the increase of both the itinerate and local moments in Fe_3GaTe_2 in view of Stoner and exchange interaction models, which results in the enhancement of the overall magnetism and a higher Curie temperature. Our work provides insight into the underlying mechanism of Fe_3GaTe_2's remarkable magnetic properties and has important implications for searching 2D materials with expected magnetic properties in the future.

DOI: 10.1088/0256-307X/40/8/087501

In recent years, research of two-dimensional (2D) van der Waals (vdW) magnetic materials, including $Cr_2Ge_2Te_6$,[1] CrI_3,[2,3] and Fe_3GeTe_2,[4,5] which exhibit rich electronic and optical properties, has opened up new avenues for exploring novel physical phenomena and applications.[6–10] The intrinsic perpendicular magnetic anisotropy (PMA) of 2D magnetic materials guarantees the existence of spin-wave gaps and stability against thermal fluctuations, thereby breaking the limitation of the Mermin–Wagner theorem and ensuring the stability of 2D long-range ferromagnetism.[1] Different from the traditional ferromagnetic materials such as $Nd_2Fe_{14}B$[11] and CoFeB,[12] 2D vdW magnetic materials are readily prepared by molecular beam epitaxial growth, which allow various stacking to form heterostructures with dangling-bond-free surfaces and easy-peel-off characteristics. Moreover, the electromagnetic transportation of 2D magnetic materials can be easily manipulated through the applications of electric gating,[3,13] pressure,[14,15] strain,[16,17] light,[18] etc. These properties make 2D magnetic materials a unique platform to investigate novel physical phenomena and to become promising candidates for next-generation spintronics.

Among numerous 2D magnetic materials, 2D ferromagnetic materials with high Curie temperature (T_c) and robust large PMA have attracted a great deal of attention for their wider applications in magnetoelectronic devices. Fe_3GaTe_2, a new 2D vdW ferromagnetic crystal, was reported last year, which can combine intrinsic above-room-temperature strong ferromagnetism ($T_c \sim 350$–$380\,K$) and robust large PMA ($\sim 4.79 \times 10^5\,J/m^3$ at $300\,K$).[19] Although the lattice structure of Fe_3GaTe_2 is similar to that of Fe_3GeTe_2 except for a little change of lattice constant, their T_c is increased from $225\,K$ of bulk Fe_3GeTe_2 to $380\,K$

*Corresponding authors. Email: qiaoshan@mail.sim.ac.cn; hxchang@hust.edu.cn
© 2023 Chinese Physical Society and IOP Publishing Ltd

of Fe_3GaTe_2. It is widely believed that Fe_3GeTe_2 is itinerant ferromagnetic metal[20] while some studies describe its magnetic properties with a Heisenberg model.[3] There is also a viewpoint that the local magnetic moments should be taken into account to understand the ferromagnetic ordering in Fe_3GeTe_2.[21] For the Fe_3GaTe_2 material, the mechanism of its highly enhanced T_c remains unknown and related studies are strongly desired.

In this work, we identify the element-resolved magnetism in Fe_3GaTe_2 using the x-ray magnetic circular dichroism (XMCD), and study the electronic structures with first-principles calculations. Compared with the reported results of Fe_3GeTe_2, the XMCD measurements show the larger magnetic moments of Fe atoms in Fe_3GaTe_2. Importantly, the Ga and Te atoms in Fe_3GaTe_2 exhibit ferromagnetism with an antiferromagnetic coupling to Fe atoms. The XMCD results are substantiated by first-principles calculations, which further reveal stronger exchange interaction between Fe and Ga atoms, accounting for the enhanced ferromagnetism. The variation in Curie temperature T_c of Fe_3GaTe_2 and Fe_3GeTe_2 can be explained by the Stoner model and exchange interaction between Fe atoms and the remained atoms.

As a powerful and effective experimental method, the XMCD can be used to investigate the spin and orbital moments of specific elements. XMCD measurements were performed at the BL07U beamline of the Shanghai Synchrotron Radiation Facility (SSRF). The sample was grown by the same method reported before.[19] The sample was post-cleaved under 10^{-8} mbar and measured under $\sim 6 \times 10^{-9}$ mbar. The sample is perpendicular to the incident synchrotron radiation. All measurements were carried out at magnetic field of 7 kOe and temperature of $T = 10$ K. The total electron yield signals of Fe L_{23} ($2p \rightarrow 3d$) absorption edges were measured with left and right circularly polarized x-rays, denoted by μ^+ and μ^- as shown in Fig. 1(a). A clear difference is observed, which indicates a strong dichroism. As shown in Fig. 1(b), the x-ray absorption spectroscopy (XAS) was obtained by $\mu^0 = (\mu^+ + \mu^-)/2$. The XAS spectrum has a step-like feature that is related to the excitation of core electrons to the continuum or quasi-continuum states.[22,23] One of the most used functions to fit the background is the double-step one with the error function erf(x):[24]

$$\begin{aligned}\text{step}(\lambda) = H_0 + mH\Big[\frac{1}{2} + \frac{1}{2}\text{erf}\Big(\frac{\lambda - \lambda_{L_3}}{\Gamma_G(L_3)\cdot\sqrt{\ln 2}}\Big)\Big] \\ + (1-m)H\Big[\frac{1}{2} + \frac{1}{2}\text{erf}\Big(\frac{\lambda - \lambda_{L_2}}{\Gamma_G(L_2)\cdot\sqrt{\ln 2}}\Big)\Big], \quad (1)\end{aligned}$$

where H represents the step height, λ_{L_i} ($i = 2, 3$) is the position of the absorption peak at different edges, Γ_G ($i = 2, 3$) is the full width at half maximum of the step, and m is the proportion of the step height corresponding to the L_3 absorption edge to the entire step height. Because the step ratio of $L_{2,3}$ edges is 2 : 1 according to their quantum degeneracies, m is determined to be 2/3.

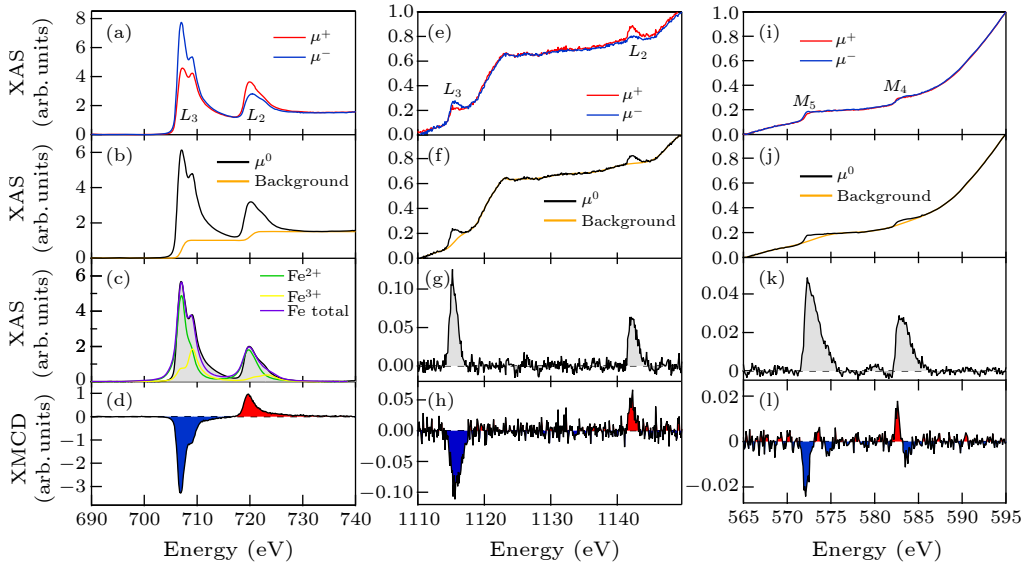

Fig. 1. Normalized XAS and XMCD spectra of Fe_3GaTe_2 at Fe L_{23}, Ga L_{23} and Te M_{45} edges. [(a), (e), (i)] Normalized XAS spectra of Fe_3GaTe_2 sample at Fe L_{23}, Ga L_{23} and Te M_{45} edges by left and right circularly polarized soft x-ray, denoted with μ^+ and μ^-, respectively. [(b), (f), (j)] Normalized XAS obtained via averaging the spectra in (a), (e), and (i), respectively. The solid orange line represents the fitting curves of the background. [(c), (g), (k)] The XAS spectra from those in (b), (f), and (j) after subtracting the background. The green, yellow and purple curves in (c) are the calculated XAS spectra of Fe^{2+}, Fe^{3+} and their summation. [(d), (h), (l)] XMCD signals $\Delta\mu = \mu^+ - \mu^-$. The data in (a) is normalized so that the edge step at L_3 is equal to 1. The data in (e) and (i) are normalized to make the intensity of the XAS spectra at 1150 eV and 595 eV to be 1.

The XAS spectrum after subtracting the background is shown in Fig. 1(c). The resulting XMCD signal is shown in Fig. 1(d) by taking the difference of the XAS spectra. To examine the possible induced magnetic moments, the XMCD spectra at the Ga $L_{2,3}$ ($2p \rightarrow 4s$) and Te $M_{4,5}$ ($3d \rightarrow 5p$) absorption edges were also measured as shown in Figs. 1(e)–1(h) and Figs. 1(i)–1(l), respectively. The background of Ga and Te spectra were obtained by poly-

nomial fitting. Although the XAS spectra only show a subtle difference in Figs. 1(e) and 1(i), the clear XMCD signals indicate the induced ferromagnetic order of Ga and Te atoms. The Fe L-edge XAS multiplet calculations were carried out by using the CTM4XAS (charge transfer multiplet for x-ray absorption spectroscopy) code to fit the experimental results as shown in Fig. 1(c). The CTM4XAS is a semiempirical program that can calculate influences of different interactions on x-ray absorption.[25] The experimental spectrum can be fitted well by the XAS from 75.3% Fe^{2+} and 24.7% Fe^{3+}. In the calculations, the slater integral reduction parameters were used and the default setting of 100% for each of these parameters is equal to 80% of the calculated Hartree–Fock values. Here, the default 100% F_{dd}, F_{pd} and G_{pd} were used, where F_{dd} and F_{pd} are the direct coulomb repulsion between $3d$ electrons and that between $3d$ and $2p$ electrons, and G_{pd} is the exchange interaction between $2p$ and $3d$ electrons. The strength of spin-orbit coupling (SOC) of $2p$ electrons was set as 105% to fit the energy difference between L_2 and L_3 edges and that of $3d$ electrons was set as 100%. Using a crystal field strength value (10 Dq) of 2 eV in the O_h symmetry, the intensity ratio of L_2 and L_3 peaks can be reproduced. Despite the Fe atoms in the sample with the C_{3v} symmetry, the O_h was chosen in the calculation because of the limitation of symmetry option in CTM4XAS. The crystal field effect in the sample is considerably weaker compared to the SOC. Moreover, C_{3v} is a subgroup of O_h. The good fitting between the theoretical results and the experimental data shows that the effect of any further splitting induced by the reduced symmetry from O_h to C_{3v} is not strong.

According to the XMCD sum rules,[26,27] the spin and orbital moments can be determined by the XAS and XMCD spectra with

$$\begin{aligned}
&\text{Fe: } \langle S_z\rangle + 7\langle T_z\rangle \\
&= (10-n)\frac{\int_{L_3}(\mu^+-\mu^-)d\omega - 2\int_{L_2}(\mu^+-\mu^-)d\omega}{\int_{L_{2,3}}(\mu^+-\mu^-)d\omega}, \\
&\langle L_z\rangle = \frac{4}{3}(10-n)\frac{\int_{L_{2,3}}(\mu^+-\mu^-)d\omega}{\int_{L_{2,3}}(\mu^+-\mu^-)d\omega}; \qquad (2)\\
&\text{Ga: } \langle S_z\rangle + 7\langle T_z\rangle \\
&= -\frac{(2-n)}{2}\frac{\int_{L_3}(\mu^+-\mu^-)d\omega - 2\int_{L_2}(\mu^+-\mu^-)d\omega}{\int_{L_{2,3}}(\mu^+-\mu^-)d\omega}, \\
&\langle L_z\rangle = 0; \qquad (3)\\
&\text{Te: } \langle S_z\rangle + 7\langle T_z\rangle \\
&= -\frac{2(6-n)}{3}\frac{\int_{M_5}(\mu^+-\mu^-)d\omega - \frac{3}{2}\int_{M_4}(\mu^+-\mu^-)d\omega}{\int_{M_{4,5}}(\mu^+-\mu^-)d\omega}, \\
&\langle L_z\rangle = -\frac{4}{3}(6-n)\frac{\int_{M_{4,5}}(\mu^+-\mu^-)d\omega}{\int_{M_{4,5}}(\mu^+-\mu^-)d\omega}. \qquad (4)
\end{aligned}$$

Here, $\langle T_z\rangle$ represents the expectation value of magnetic dipole contribution and is usually negligible for bulk materials,[28] n is the electron occupation number of the final states, $\langle S_z\rangle$ and $\langle L_z\rangle$ are the expectation values of spin and orbital moments. The spin and orbital magnetic moments m_{spin} and m_{orb} are equal to $-2\langle S_z\rangle\mu_{\text{B}}$ and $-\langle L_z\rangle\mu_{\text{B}}$, respectively. According to the DFT calculations as discussed below, the electron occupation numbers of Fe, Ga, and Te atoms in Fe_3GaTe_2 are 6.3, 1.4, and 2.0, respectively.

According to the above equations, the spin moments in Fe_3GaTe_2 are calculated from the experimental XMCD spectra to be 1.82 μ_{B}/atom, $-0.34\,\mu_{\text{B}}$/atom, $-0.40\,\mu_{\text{B}}$/atom for Fe, Ga, and Te atoms, respectively, while the orbital moments of Fe, Ga, and Te atoms are calculated to be 0.37 μ_{B}/atom, 0 μ_{B}/atom, and $-0.31\,\mu_{\text{B}}$/atom, respectively. It is noteworthy that the magnetic moments of Ga and Te atoms are antiparallel to those of Fe atoms. The total magnetic moment of one Fe_3GaTe_2 molecule can be estimated to be 4.83 μ_{B} and the total moment averaged to single Fe atom is 1.61 μ_{B}, which agrees well with the experimental result of 1.68 μ_{B}/Fe[19] observed by a vibrating sample magnetometer where the magnetic moment was supposed from Fe atoms only. The XMCD results indicate the significant contribution from Ga and Te atoms to the total magnetic moment, which shows the strong magnetic couplings between Ga and Te/Fe atoms in Fe_3GaTe_2.

To examine the mechanism of enhanced magnetism in Fe_3GaTe_2, first-principles calculations are performed. First-principles calculation was performed using Vienna *ab initio* simulation package (VASP)[29,30] and WannierTools.[31] The local density approximation exchange-correlation functions[32] were chosen to calculate the magnetic moment. For both calculations of Fe_3GaTe_2 and Fe_3GeTe_2, the same pseudopotential was applied. The cutoff energy for the plane-wave basis was set as 480 eV.

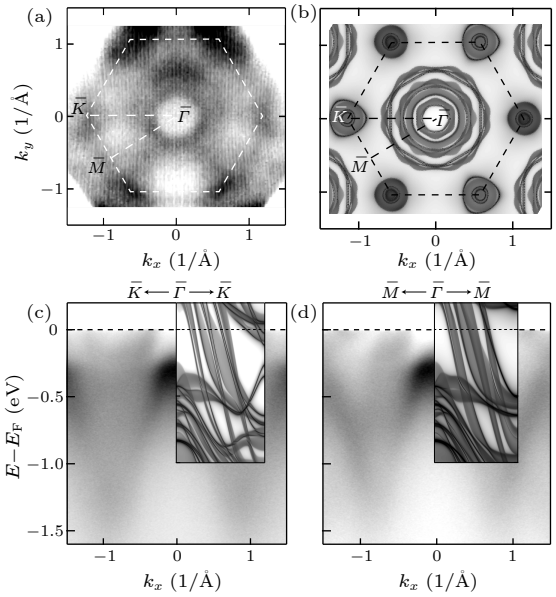

Fig. 2. The experimental and calculated electronic structure of Fe_3GaTe_2. (a) The experimental Fermi surface. (b) The theoretical Fermi surface. [(c), (d)] The experimental bands along $\bar{\Gamma}$–$\bar{K}$ and $\bar{\Gamma}$–$\bar{M}$ directions. The insets in (c) and (d) are the corresponding theoretical ones.

To check the correctness of the calculations. The electronic structure of Fe_3GaTe_2 was obtained by angle-resolved photoelectron spectroscopy (ARPES) and compared with the theoretical results. In the calculations, the ferromagnetic electronic structure was obtained by setting all the Fe atoms to align ferromagnetically. The self-consistent calculations reveal that the total magnetic moment of bulk Fe_3GaTe_2 per Fe atom is 1.76 μ_{B}, which agrees well with the experimental data and the theoretical

results reported before.[33] ARPES spectra were measured at the BL03U beamline of the SSRF with 114 eV photons. Sample temperature was kept at 21 K to ensure the sample in the ferromagnetic state in the experiment. Theoretical results match with the experimental data well as shown in Fig. 2. On the Fermi surface as shown in Figs. 2(a) and 2(b), a hexagonal hole pocket with a complex texture structure can be seen at the $\bar{\Gamma}$ point and a small electron pocket can be seen at the $\bar{K}$ point after compared with the band dispersions along high symmetry paths.

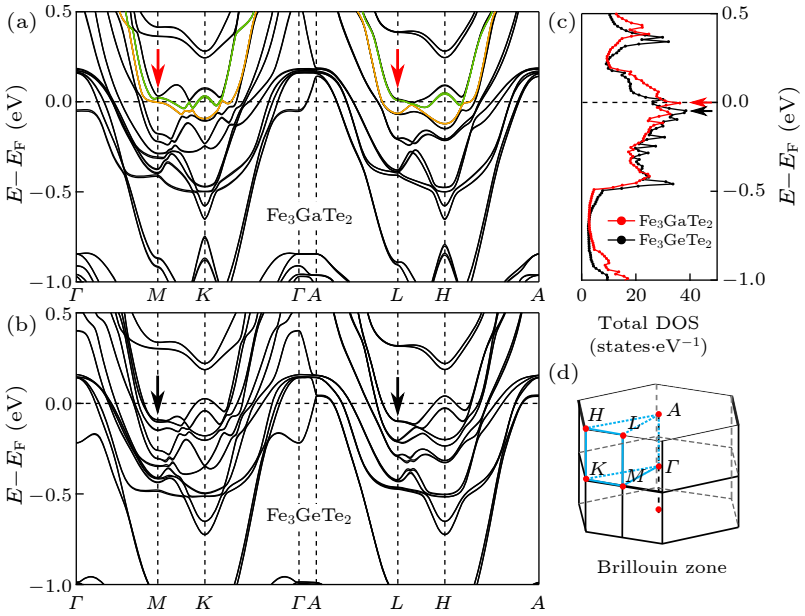

Fig. 3. The calculated non-magnetic bands and density of states (DOS) of bulk Fe_3GeTe_2 and Fe_3GaTe_2. [(a), (b)] Band structures of Fe_3GaTe_2 and Fe_3GeTe_2, respectively. Green and orange lines represent the bands having singularities at the Fermi level in Fe_3GaTe_2. The red and black arrows mark the positions of van Hove singularities in two materials. (c) The total DOS of two materials as a function of energy. The extreme DOSs are marked by red and black arrows corresponding to the singularities in (a) and (b), respectively. (d) The Brillouin zone and high-symmetry k paths of both the materials.

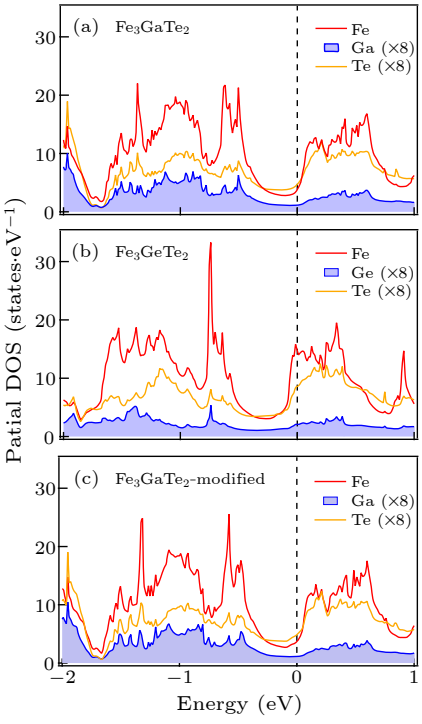

Fig. 4. The ferromagnetic partial DOSs of Fe_3GaTe_2, Fe_3GeTe_2, and modified Fe_3GaTe_2 in a unit cell. For clear comparison, the DOSs of Ga, Ge and Te are multiplied by 8 times and the DOSs of Ga/Ge are marked by blue areas.

The calculated non-magnetic band structures of bulk Fe_3GaTe_2 and Fe_3GeTe_2 are shown in Figs. 3(a) and 3(b). Notably, van Hove singularities at M and L points are observed at the Fermi level for Fe_3GaTe_2 as shown in Fig. 3(a) marked by orange and green lines, respectively, while the corresponding bands of Fe_3GeTe_2 are at a binding energy of 0.1 eV. The singularities at Fermi energy render the electronic state of Fe_3GaTe_2 unstable, leading to the easy development of ferromagnetic order. The non-magnetic DOSs of the two materials shown in Fig. 3(c) are similar near the Fermi level, except for the slight shift of Fe_3GaTe_2's to the high energy side, which can be attributed to the one electron less for Ga than Ge. Obviously, the DOS of Fe_3GaTe_2 exhibits an extremum at the Fermi level, caused by the presence of van Hove singularities. There is an itinerate model called the Stoner model with a Stoner criterion to evaluate whether spontaneous magnetism can be formed. According to the Stoner criterion,[34] if $U \cdot D_{\rm NM}(E_{\rm F}) > 1$, the ferromagnetism of the material can be formed, where U represents the Hubbard U, and $D_{\rm NM}(E_{\rm F})$ represents the non-magnetic DOS at Fermi level $E_{\rm F}$. Based on the Stoner model, it is commonly inferred that the DOS near the Fermi level plays a crucial role in determining the Curie temperature of a material. Specifically, it is believed that the larger the DOS near the Fermi level is, the higher the Curie temperature should be for a certain Hubbard U. Returning to the DOS spectra depicted in Fig. 3(c), it becomes apparent that the significant variation in Curie temperature

between the Fe_3GeTe_2 and Fe_3GaTe_2 can be explained by the Stoner model with different DOSs at E_F.

The ferromagnetic partial DOS of Fe_3GaTe_2 and Fe_3GeTe_2 in a unit cell are shown in Figs. 4(a) and 4(b). The DOS intensities of Fe of the two materials are similar except the sharp peak around 0.74 eV binding energy, while the DOS of Ga is much higher than that of Ge, suggesting the stronger hybridization between Ga and Fe atoms. In order to exclude the possibility that the stronger hybridization in Fe_3GaTe_2 caused by its smaller lattice constant, its partial DOS with the lattice constants of Fe_3GeTe_2 was calculated as shown in Fig. 4(c). The partial DOSs of Fe_3GaTe_2 with different lattice constants are almost same as shown in Figs. 4(a) and 4(c), therefore the stronger hybridization between Fe and Ga atoms is not due to the smaller lattice constant.

In summary, we have utilized XMCD to investigate the orbital and spin magnetic moments of different elements in 2D vdW ferromagnetic material Fe_3GaTe_2. Our results show that both Ga and Te atoms have induced ferromagnetic moments and contribute significantly to the total magnetic moments, which means the existence of strong magnetic couplings between Fe and Ga/Te atoms. Our results also show the antiferromagnetic couplings between Fe and Ga/Te atoms. Additionally, the first-principles calculations reveal that although the Ga atom has only one electron less than the Ge atom, it leads to van Hove singularities in the non-magnetic DOS at the Fermi level, making Fe_3GaTe_2 in a metastable state and more susceptible to form ferromagnetic order. Moreover, our calculations show a stronger hybridization between Ga and Fe atoms, which strengthens the exchange interaction between Fe atoms, ultimately enhancing the ferromagnetism of the system with a higher Curie temperature in Fe_3GaTe_2.

Acknowledgments. This work was supported by the National Key R&D Program of China (Grant Nos. 2022YFB3608000 and 2022YFE0134600), the National Natural Science Foundation of China (Grant Nos. U1632266, 11927807, U2032207, and 52272152). The ARPES experiments were performed with the approval of the Proposal Assessing Committee of SiP·ME2 platform project (Proposal No. 11227902). We thank the staff at the BL07U beamline of Shanghai Synchrotron Radiation Facility (SSRF) for assistance of XMCD/XAS data collection.

References

[1] Gong C, Li L, Li Z, Ji H, Stern A, Xia Y, Cao T, Bao W, Wang C, Wang Y, Qiu Z Q, Cava R J, Louie S G, Xia J, and Zhang X 2017 *Nature* **546** 265
[2] Huang B, Clark G, Navarro-Moratalla E, Klein D R, Cheng R, Seyler K L, Zhong D, Schmidgall E, McGuire M A, Cobden D H, Yao W, Xiao D, Jarillo-Herrero P, and Xu X 2017 *Nature* **546** 270
[3] Lado J L and Fernández-Rossier J 2017 *2D Mater.* **4** 035002
[4] Deng Y J, Yu Y J, Song Y C, Zhang J Z, Wang N Z, Sun Z, Yi Y F, Wu Y Z, Wu S W, Zhu J Y, Wang J, Chen X H, and Zhang Y B 2018 *Nature* **563** 94
[5] Fei Z Y, Huang B V, Malinowski P, Wang W B, Song T C, Sanchez J, Yao W, Xiao D, Zhu X Y, May A F, Wu W, Cobden D H, Chu J H, and Xu X D 2018 *Nat. Mater.* **17** 778
[6] Song T C, Cai X H, Tu M W Y, Zhang X O, Huang B V, Wilson N P, Seyler K L, Zhu L, Taniguchi T, Watanabe K, McGuire M A, Cobden D H, Xiao D, Yao W, and Xu X 2018 *Science* **360** 1214
[7] Klein D R, MacNeill D, Lado J L, Soriano D, Navarro-moratalla E, Watanabe K, Taniguchi T, Manni S, Canfield P, Fernández-rossier J, and Jarillo-herrero P 2018 *Science* **360** 1218
[8] Arai M, Moriya R, Yabuki N, Masubuchi S, Ueno K, and Machida T 2015 *Appl. Phys. Lett.* **107** 103107
[9] Kim H H, Yang B, Patel T, Sfigakis F, Li C, Tian S, Lei H, and Tsen A W 2018 *Nano Lett.* **18** 4885
[10] Wang Z, Zhang T, Ding M, Dong B, Li Y, Chen M, Li X, Huang J, Wang H, Zhao X, Li Y, Li D, Jia C, Sun L, Guo H, Ye Y, Sun D, Chen Y, Yang T, Zhang J, Ono S, Han Z, and Zhang Z 2018 *Nat. Nanotechnol.* **13** 554
[11] Givord D, Li H S, and Moreau J M 1984 *Solid State Commun.* **50** 497
[12] Ikeda S, Miura K, Yamamoto H, Mizunuma K, Gan H D, Endo M, Kanai S, Hayakawa J, Matsukura F, and Ohno H 2010 *Nat. Mater.* **9** 721
[13] Verzhbitskiy I A, Kurebayashi H, Cheng H, Zhou J, Khan S, Feng Y P, and Eda G 2020 *Nat. Electron.* **3** 460
[14] Song T C, Fei Z Y, Yankowitz M, Lin Z, Jiang Q N, Hwangbo K, Zhang Q, Sun B S, Taniguchi T, Watanabe K, McGuire M A, Graf D, Cao T, Chu J H, Cobden D H, Dean C R, Xiao D, and Xu X 2019 *Nat. Mater.* **18** 1298
[15] Li T X, Jiang S W, Sivadas N, Wang Z F, Xu Y, Weber D, Goldberger J E, Watanabe K, Taniguchi T, Fennie C J, Fai M K, and Shan J 2019 *Nat. Mater.* **18** 1303
[16] Wang Y, Wang C, Liang S J, Ma Z, Xu K, Liu X, Zhang L, Admasu A S, Cheong S W, Wang L, Chen M, Liu Z, Cheng B, Ji W, and Miao F 2020 *Adv. Mater.* **32** 2004533
[17] Hu L, Zhou J, Hou Z, Su W, Yang B, Li L, and Yan M 2021 *Mater. Horiz.* **8** 3306
[18] Liu B, Liu S, Yang L, Chen Z, Zhang E, Li Z, Wu J, Ruan X, Xiu F, Liu W, He L, Zhang R, and Xu Y 2020 *Phys. Rev. Lett.* **125** 267205
[19] Zhang G, Guo F, Wu H, Wen X, Yang L, Jin W, Zhang W, and Chang H 2022 *Nat. Commun.* **13** 5067
[20] Chen B, Yang J, Wang H, Imai M, Ohta H, Michioka C, Yoshimura K, and Fang M 2013 *J. Phys. Soc. Jpn.* **82** 124711
[21] Xu X, Li Y W, Duan S R, Zhang S L, Chen Y J, Kang L, Liang A J, Chen C, Xia W, Xu Y, Malinowski P, Xu X D, Chu J H, Li G, Guo Y F, Liu Z K, Yang L X, and Chen Y L 2020 *Phys. Rev. B* **101** 201104
[22] Chen C T, Idzerda Y U, Lin H J, Smith N V, Meigs G, Chaban E, Ho G H, Pellegrin E, and Sette F 1995 *Phys. Rev. Lett.* **75** 152
[23] Dunn J H, Arvanitis D, Martensson N, Tischer M, May F, Russo M, and Baberschke K 1995 *J. Phys.: Condens. Matter* **7** 1111
[24] Chen J G 1997 *Surf. Sci. Rep.* **30** 1
[25] Stavitski E and De Groot F M F 2010 *Micron* **41** 687
[26] Thole B T, Carra P, Sette F, and van der Laan G 1992 *Phys. Rev. Lett.* **68** 1943
[27] Carra P, Thole B T, Altarelli M, and Wang X 1993 *Phys. Rev. Lett.* **70** 694
[28] Wu R and Freeman A J 1994 *Phys. Rev. Lett.* **73** 1994
[29] Kresse G and Furthmüller J 1996 *Phys. Rev. B* **54** 11169
[30] Kresse G and Furthmüller J 1996 *Comput. Mater. Sci.* **6** 15
[31] Wu Q S, Zhang S N, Song H F, Troyer M, and Soluyanov A A 2018 *Comput. Phys. Commun.* **224** 405
[32] Perdew J P, McMullen E R, and Zunger A 1981 *Phys. Rev. A* **23** 2785
[33] Li X L, Zhu M, Wang Y Y, Zheng F X, Dong J T, Zhou Y, You L, and Zhang J 2023 *Appl. Phys. Lett.* **122** 082404
[34] Blundell S and Thouless D 2003 *Am. J. Phys.* **71** 94